

# A Comparison of 3 Digital Image Correlation Techniques on Necessarily Suboptimal Random Patterns Recorded By X-Ray

P.J. Rae · D.M. Williamson · J. Addiss

Received: 6 August 2010 / Accepted: 17 November 2010 / Published online: 14 December 2010  
© Society for Experimental Mechanics 2010

**Abstract** Dynamic x-rays have been used to follow the deformation ahead of a steel ball fired into a mock-up of a generic cylindrical rocket motor. The impact was arranged to intersect a sparse lead powder layer within the mock explosive that created a random speckle pattern on x-ray film. Three different digital image correlation programs are compared to examine any sensitivity to the sub-optimal speckle pattern produced by the lead powder. An identical output data reduction method was used in all cases to aid comparison. All three correlation methods were able analyze the deformation, but all had intricacies that would require more detailed optimization of the data reduction in order to fully exploit the technique. Quantitative analysis showed that the three methods agreed closely in estimations of rigid body displacements between a pair of representative x-ray images. It was discovered that the deformation caused by the ball impact was highly localized and the useful data available about the deformation pattern was sparse. This limits the applicability of this technique to this specific application. Extensive cracking was not

observed that would have aided the development of computer-based models for prediction of such impact events. The x-ray technique was however excellent for determining the ball position as a function of time after impact.

**Keywords** Image correlation · X-ray · Propellant · Deformation · Fragment attack

## Introduction

The advent of personal computers has allowed the development of digital image correlation techniques to extract information about object motion and deformation from two or more images between which displacement has occurred. This technique is particularly suited to objects that already have, or can have added, a random pattern that can be imaged by some means. The technique has been widely used in the field of experimental mechanics [1].

Numerous algorithms have been published to perform the digital correlation, however, fundamentally they all work in a similar manner. An object that will undergo some form of deformation is photographed before the start of the experiment and then a sequence of images is recorded during deformation. By selecting small sub-images from the undeformed and deformed images and mathematically comparing them, a best-fit displacement in pixels can be found that maps one onto the other. By repeating this process over the whole image and suitably scaling the answers, a whole field displacement map in SI units can be created. It is useful if the pattern recorded is random because this likely provides a single correlation peak. Repeating

---

P.J. Rae (✉)  
Los Alamos National Laboratory,  
Los Alamos, NM 87545, USA  
e-mail: prae@lanl.gov

D.M. Williamson · J. Addiss  
Department of Physics, Cavendish Laboratory,  
University of Cambridge, J J Thomson Avenue,  
Cambridge, CB3 0HE, UK

D.M. Williamson  
e-mail: dmw28@cam.ac.uk

J. Addiss  
e-mail: ja304@cam.ac.uk



patterns, such as grids, can be used but the magnitude of displacement to be followed is limited because the correlation algorithm may find multiple peaks if the search area becomes too large.

In general, white light or laser speckle images are recorded from the surface of the object either to film or directly to electronic imaging chips. By recording the images stereoscopically, out of plane motions may be resolved. One obvious method of obtaining deformation fields from within objects rather than just surface displacements is to use x-rays. This potentially powerful technique has some limitations however. Firstly a means of x-ray contrast must be introduced and this is difficult to achieve in metallic objects greater than a few millimeters in thickness. This limits the technique to relatively low atomic number materials (sand, concrete, polymers etc.). Secondly, the contrast layer is necessarily a different material from the bulk and may influence the displacement. Finally, from a practical point of view, it is much harder to add an optimal speckle pattern inside an object and there are issues with the finite spot size of the x-ray head then blurring the image.

It has been shown that the optimum speckle size for laser based image correlation is greater than 1 pixel but is much smaller than a  $2 \times 2$  pixel array [2]. For white light speckles it has been found that this increases to around  $3.5 \times 3.5$  [3]. For the majority of experiments undertaken using image correlation, the random pattern is added using contrasting spray paint (typically a white background is added and black speckles are sprayed on). In the hands of a careful experimenter, the size of the speckles may be closely controlled and optimized for a given object and field of view. This is optimization is much harder to achieve with x-ray contrast materials embedded in the test object.

There is significant interest in improving the safety of missile motor bodies to accidental fragment attack. Missile propellants generally fall into two classes, those where the main ingredient is ammonium perchlorate (AP) and the so-called 'min smoke' (minimal smoke producing) propellants that typically use molecular explosive solids such as HMX and RDX in a burning mode to produce thrust. A high velocity fragment striking a missile body may induce burning of the propellant. The desired result is that this burning self quenches before a large-scale accident happens. In AP based propellants the large-scale event is generally rapid burning of the propellant and unpredictable and rapid motion of the motor. Burning in 'min smoke' propellants may lead to a DDT event (deflagration to detonation) that produces further fragments and widespread damage [4]. The propellants typically comprise of a high volume fraction of particles of reactive material held

in a soft rubber binder. The motor has a hole down the middle that allows propagation of the burning and may be a complex shape in real motors. The propellant is held inside a casing by a thin thermally insulating layer of rubber. The casing material can be metallic or a polymer composite. The composite cases are generally preferred in modern systems because they burst more easily under pressurization from accidental causes, but function correctly when intentionally lit. Early bursting of the case usually reduces the severity of an accident.

Understanding the behavior of rocket motor to accidental fragment attack is complicated by being coupled physics. The fragment causes a shock wave and extensive rapid deformation (often largely shear). Assuming the shock is not strong enough to lead to prompt initiation, the process causes heating adding additional energy to the propellant now possibly with a hot lodged metal fragment. This heating causes chemical reaction of the propellant that causes gas pressurization and therefore faster burning. What happens next is a complex combination of geometry, strength of materials, inertial and physical confinement, burning behavior and statistics. The outcome can be very different depending if the hot fragment is stopped before the central burn core, or if it crosses the burn hole before stopping or if it actually penetrates the full diameter of the motor and does not remain embedded.

The purpose of this proof of principal study was to use x-ray speckle image correlation to measure the displacement ahead of a spherical projectile being fired at a mock (non-reactive) motor casing. The mock motor was made using 6061-aluminum tubing, a Sylgard 184 rubber insulation layer and a mock explosive (PBS 9501) with a central round 'burn' hole. The materials were chosen to simplify eventual computer modeling of the experiment for later computer code verification because material equations of state and strength models exist for these substances. Running computer simulations on a mock material simplifies the problem but exercises the strength and equation of state assumptions used.

## Experimental

### Impacts

Here the mock propellant is really a mock explosive. It was chosen because a mock propellant was not readily available in a form that would allow the inclusion of a lead powder. Additionally a strength model and equation of state for PBS 9501 has already been developed. PBS 9501 is 94% by weight sugar (3:1 sieve cut giving



an approximate bimodal distribution with peaks at 100 and 20  $\mu\text{m}$ ) with 3% Estane rubber and 3% BDNPAF plasticizer. A small fraction of red dye is also included to indicate that it is a mock explosive. The binder is dissolved in excess ethyl acetate before adding the sugar. The sugar powder is evenly coated with binder by mixing before the solvent is driven off by stirring, heating and the application of vacuum. The resulting molding powder (prills) range in size from dust to pea sized lumps. PBS 9501 is a mechanical properties stimulant for a LANL explosive, PBX 9501 [4].

To manufacture the mock propellant cores, 62 g of molding powder heated to 125°C was added and lightly tamped into a 58 mm diameter die also preheated to 125°C. Lead particles were poured in to form a sparse layer prior to another 62 g of molding powder. The puck was pressed to consolidation by the application of 20,000 kg. The one-dimensional stress reached was approximately 76 MPa. This is about half the stress reached when real PBX 9501 is pressed (140 MPa, 20,000 psi), however the PBS was heated to 125°C rather than the usual 100–105°C further softening the binder. The pressed density of 1539  $\text{kg m}^{-3}$  was calculated by measuring the volume of the finished puck and from mass of mock used. The density of crystalline sugar is 1586  $\text{kg m}^{-3}$  and the binder 1270  $\text{kg m}^{-3}$  resulting in a TMD (theoretical maximum density) of 1567  $\text{kg m}^{-3}$ . It therefore appears that the PBS 9501 was pressed to 98.5% of TMD, a similar value to real PBX 9501. Note that the density of HMX, the real explosive in PBX 9501 is approximately 1900  $\text{kg m}^{-3}$  resulting in a TMD of 1860  $\text{kg m}^{-3}$ , so the sugar mock is slightly less dense than real explosive.

Two propellant cores were made, ones that were solid and ones with a 24 mm diameter hole through the middle to represent a burn core. The mock samples were potted into 6061 aluminum tubes to represent a motor casing with Sylgard 184 silicone rubber. The rubber was mixed at the recommended 10:1 precursor to cure agent ratio and placed in an oven at 50°C for 12 hours to cure.

The lead layer was made two ways. The first method tried was to use Sigma Aldrich lead particles less than 1.5 mm in diameter (part number 396117-2kg). This was found to give unacceptably large, but crisp, speckles. A second method used a non-contiguous layer of Sigma lead granules (part number 11502) together with about the same mass of Sigma 396117 larger ones. This resulted in more satisfactory speckles for image correlation purposes.

Three designs of target are reported here, the first solid design had no central burn hole and used only larger lead particles. The second solid design used the

mix of particles but also had no burn hole, and finally the third had the mix of lead particles and the central burn hole creating a ring. Figure 1 shows a sketch and dimensions of the target design and Fig. 2 shows a photograph with the make trigger circuit attached to the outside for timing and triggering purposes. In the sample photograph the lead layer is just visible as a dark ring inside the burn hole. The arrangement of the experiment is shown in Fig. 3.

The impacts were recorded on a Scandiflash 150 keV x-ray system using Agfa Curix Ortho Regular intensifier plates and Agfa Curix HT1.000G Plus film (180  $\times$  240 mm), developed in open baths with Agfa Dentus D developer and Agfa Dentus F fixer. The x-ray flash system produces a pulse width of less than 70 ns with a spot size of better than 3 mm. The system employs a step up transformer on the output so that charging the capacitors to 30 keV produces 150 keV at the tube. All experiments reported used lower energy x-rays than this by charging the capacitors to 18 keV.

The projectiles were 8 mm hardened steel ball bearings shot from a helium driven gun. A firing pressure of 39 bar was found to give a fairly reproducible muzzle velocity of 490  $\text{m s}^{-1}$ . The velocity was measured by the projectile interrupting two laser beams 19.70 mm apart. The targets were aligned in front of the muzzle so the projectile hit across a diameter and at the lead layer. The target was not restrained in the direction of the projectile and so moved as momentum was transferred.

A Scandiflash delay generator was used to delay the x-ray exposure after the projectile reached the target.

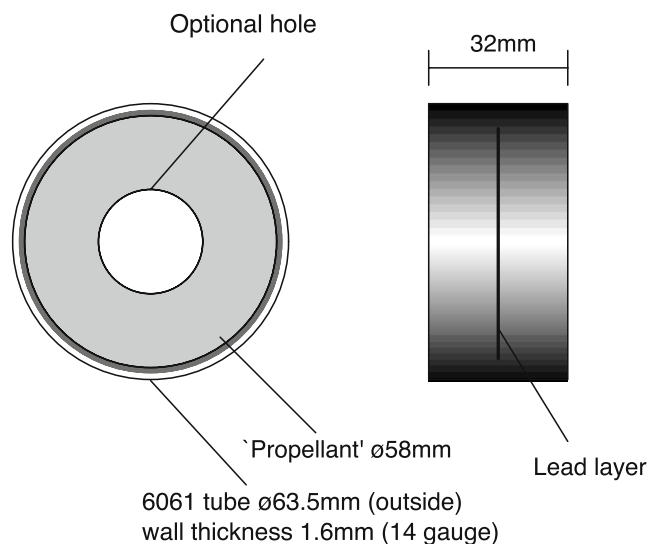


**Fig. 1** The dimensions of the samples. The gray band between the 'propellant' and the tube is Sylgard 184 silicone rubber potting material



**Fig. 2** A photograph of a ring sample with the make-foil gauge attached

The arrival was accurately indicated by the steel ball shorting out a thin flexible Mylar/copper printed circuit tape bonded to the aluminum tube. In this way velocity jitter from the gun did not affect the real exposure delay into the target. Analysis of the recovered balls showed no fracture or plastic deformation. Therefore, in all modeling simulations the hardened steel may be regarded as a purely elastic material.

### Correlation Techniques

Many methods of digital image correlation have been published and they vary greatly in complexity. Broadly,

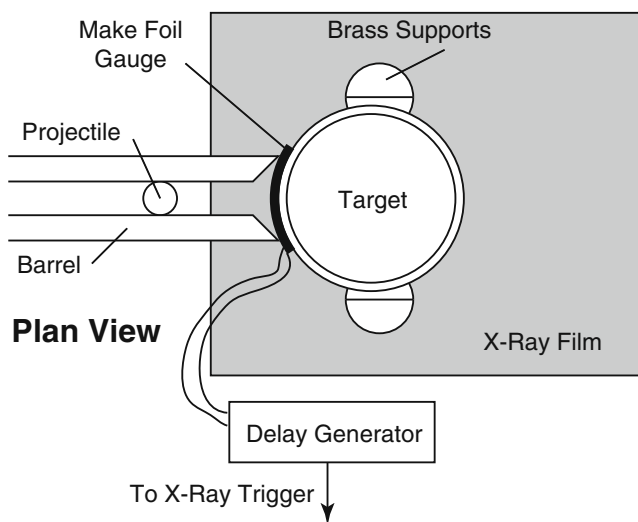


**Fig. 3** A schematic of the experimental arrangement

two approaches are taken, correlation in the spatial domain [5–8] and in the frequency domain [2, 9–12]. Historically, the frequency domain methods were used because they resulted in significantly faster running code than methods working in the spatial domain, however, owing to the vast increase in speed of desktop computers in the last 20 years, this is less of a practical issue than it used to be. The advantage of the spatial domain is that rotation and shear of the correlation sub-images can be directly measured, this is not possible in the frequency domain.

Three correlation techniques were used on the x-ray images for comparison. The x-ray images, as previously described, are not easy to optimize in terms of the speckle size and contrast. It was therefore not clear which method, if any, would perform best.

Processed x-ray films were scanned using a backlit Epson V750 scanner in 8-bit grayscale mode. Only 8-bits were used since two of the analysis methods are only capable of processing 8-bit grayscale images. Ideally, a greater dynamic range would be used since it has been shown to be advantageous [13]. The scanned images were saved as lossless TIFF images for later analysis. The scanner was run in basic mode with no automatic image ‘enhancement’ performed.

Method 1 used the Vic-2D commercial software<sup>1</sup> which is a highly developed and refined version of reference [8] and [5]’s method of correlation in the spatial domain. Method 2 is due to Sjö Dahl and makes use of the FFT (fast Fourier transform) in the frequency domain and has been termed DIC (digital image correlation). Sophisticated sub-pixel image shifting is performed to optimize the overlap between sub-images resulting in increased accuracy in an optimized speckle pattern. Method 3 also used the FFT to perform the correlation, however, a simple bi-cubic is fit to the maximum correlation peak to find the average displacement between sub-images [14]. This has been termed PIV (particle image velocimetry) because it was originally designed for tracking particles in a fluid flow. One advantage of Method 3 is that a bigger area is automatically searched for a correlation peak without an initial guess being supplied by the user than the other two techniques. This allows larger rigid body deformations between frames to be followed if not too much image detail change has occurred.

All correlation methods produced an output file containing, amongst other data, the pixel displacement estimate from a location in the reference image to

<sup>1</sup>[www.correlatedsolutions.com](http://www.correlatedsolutions.com)

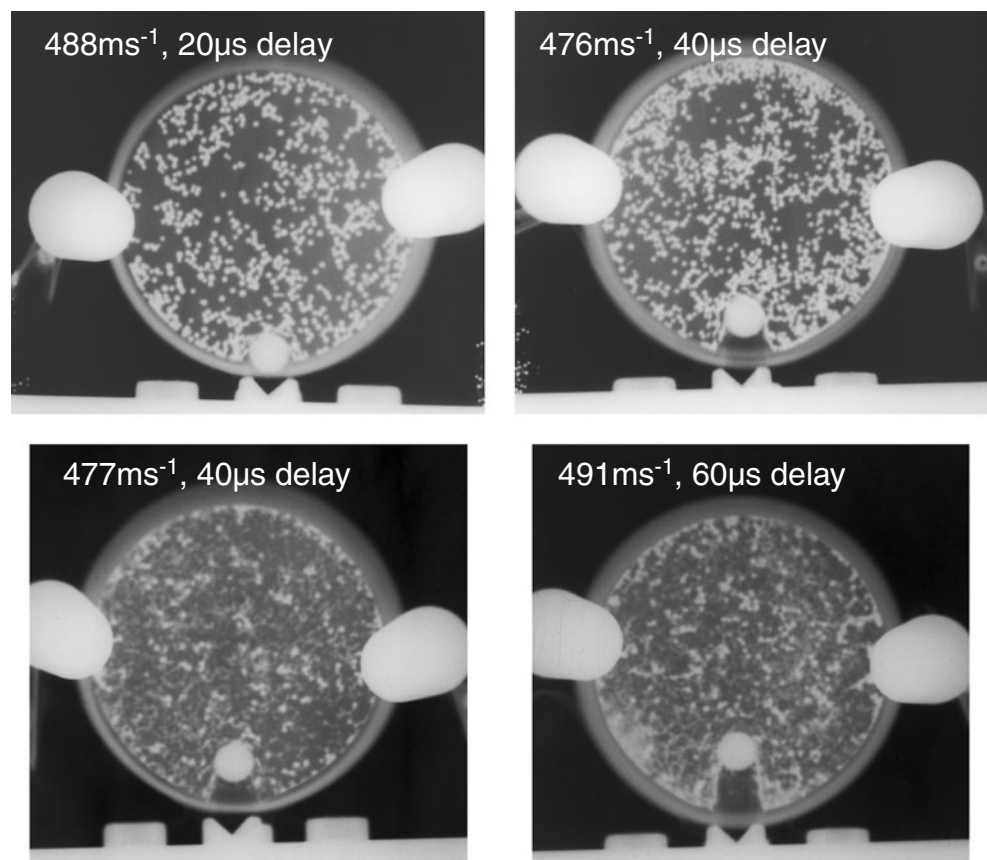
the displaced one. They also all outputted some metric describing the correlation peak magnitude which is a measure of the similarity of the image segments. The method of calculating the correlation coefficient differed in the codes and so a constant cutoff value for the magnitude of the correlation peak could not be used for all three. This aspect is discussed more fully later.

The data reduction and presentation was done using MATLAB software. After loading the displacements text file, the displaced image upon which to overlay a ‘quiver’ plot (a grid of scaled vector arrows showing displacement from a starting point) was loaded. Outlying displacements were trimmed first by analyzing the maximum displacements found ahead of the ball to the nearest pixel. Displacements larger than that were subsequently ignored during correction. The aim was to preserve all possible valid data but remove rogue points. The data were corrected for both rigid body displacement and rigid body rotation by considering an essentially undeformed region of speckle pattern well in front of the projectile close to the rear casing. It was assumed that this region saw insignificant deformation but representative rigid body motion. From performing image correction analysis of this location a 2D rigid

body and rigid rotation was calculated and the result subtracted over the whole field of view. This process improves the aesthetic look of the plots, but also allows the relatively small and real displacements to be seen in the presence of larger rigid displacements. Finally, an arbitrary displacement cutoff in the horizontal and vertical directions was chosen for the shots. Displacements larger than the chosen value were set to zero to remove any remaining rogue points. The same cut-off value was used for the results of the three methods. The corrected displacements were magnified by 3 in the quiver plot and overlaid on the scaled x-ray images.

Some of this data filtering was required because regions of interest were electronically cropped by eye from the full sized x-ray images. This resulted in significant rigid body displacements between the reference and dynamic images. If these rigid body displacements were not removed, determining the relatively small differences caused by the ball motion in the quiver plots would have been difficult. In many modern flash x-ray systems, electronic phosphor plates are used allowing almost perfect registration of images between frames, however this was not available for these experiments.

**Fig. 4** X-rays taken during impact into solid targets. The delay from the ball touching the aluminum ring is shown together with the velocity of the ball prior to contact





## Results

Experiments were repeated for both the solid and ring targets with differing delay time after ball contact with the aluminum outer ring. In this way a sequence of penetration magnitudes were recorded for comparison with any later computer modeling of the geometry. Figure 4 shows impacts at differing delays from aluminum ring

contact into solid targets and Fig. 5 shows impacts into ring targets.

The white object on the right and left of the samples are brass cylinders used to lightly support the assembly. The angular beam expansion and the depth effect makes them appear non-circular in the x-rays. Considering Fig. 4, it is seen that the top two samples had only the larger lead spheres, while the bottom two had the

**Fig. 5** X-rays taken during impact into ring targets. The delay from the ball touching the aluminum ring is shown together with the velocity of the ball prior to contact

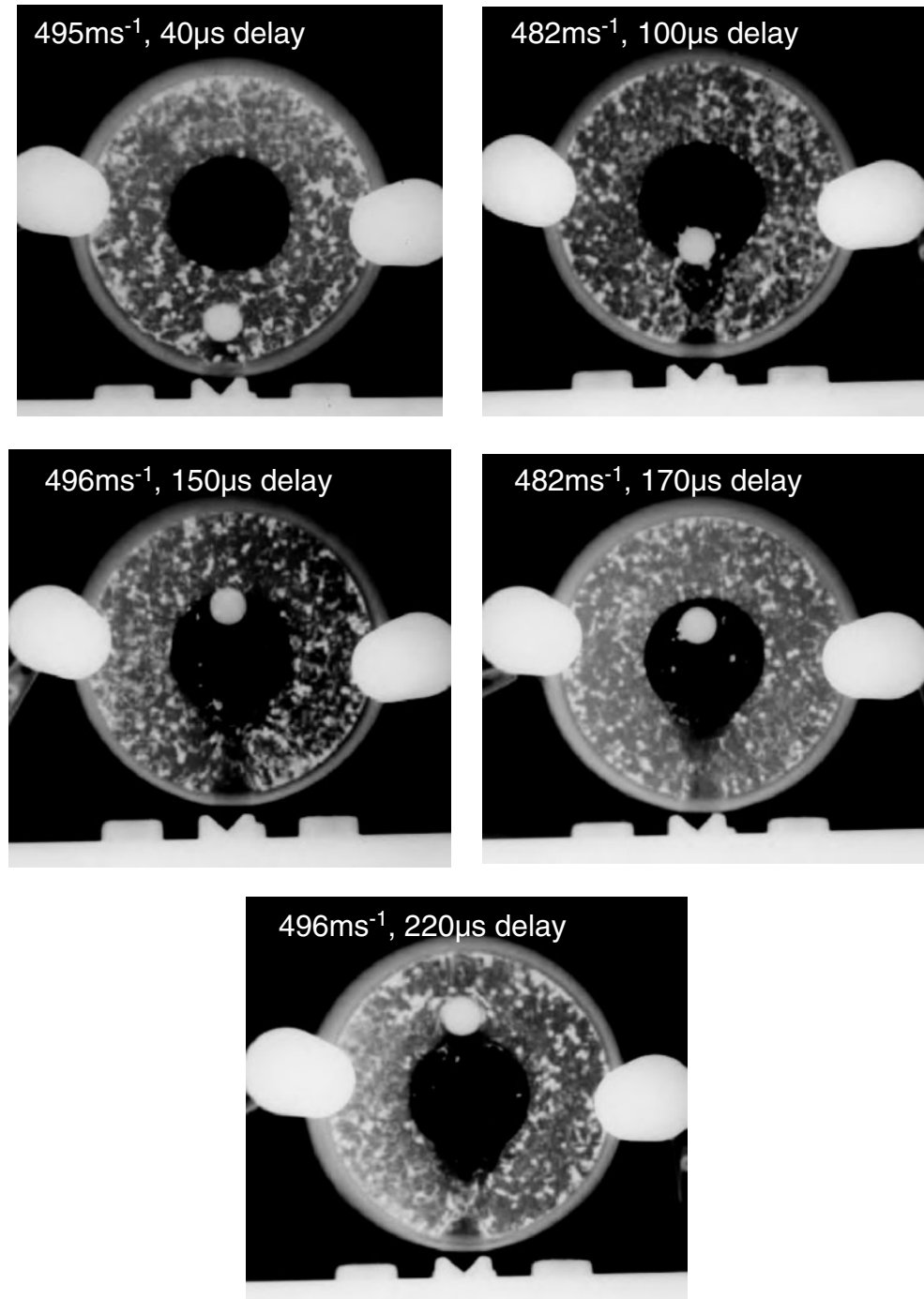


**Table 1** The sample window sizes and steps used in the calculations for the two samples and three codes

Code	Solid sample / pixels	Ring sample / pixels
VIC (1)	101 × 101 step 32	65 × 65 step 32
DIC (2)	128 × 128 step 32	64 × 64 step 32
PIV (3)	128 × 128 step 32	64 × 64 step 32

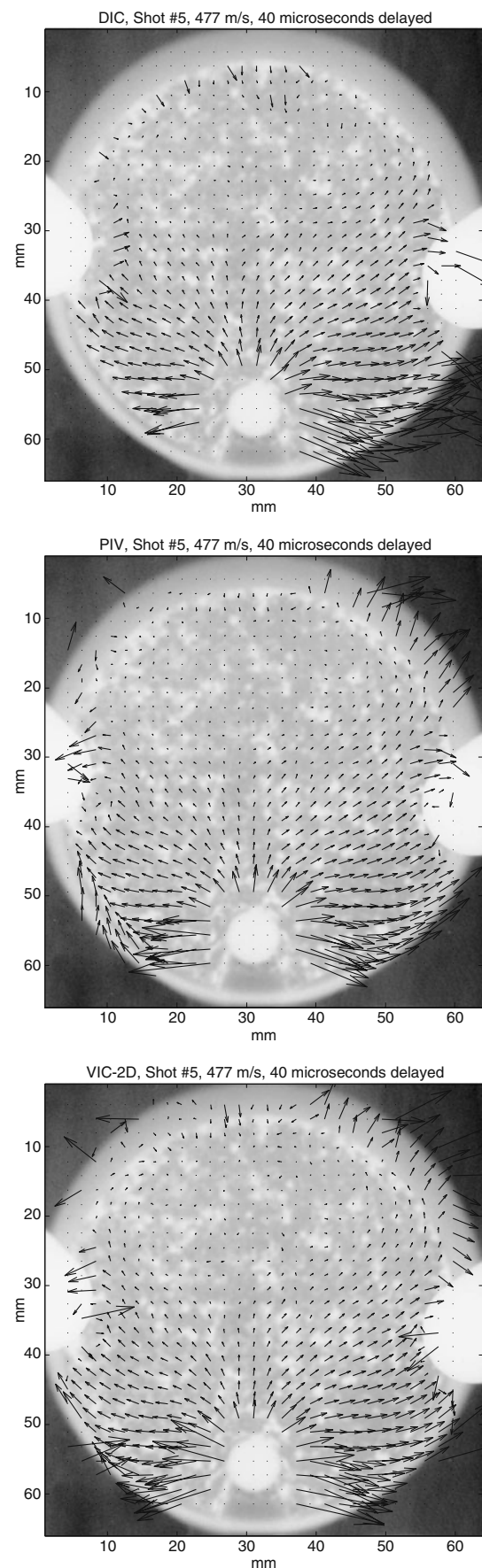
particle size distribution. The ball quickly slowed in the mock in the solid geometry and remain lodged in most solid sample tests. As expected, the penetration in the ring geometry was greater and resulted in greater fragmentation of the sample. The gun exhibited a certain velocity jitter and it will be observed in Fig. 5 that the ball has progressed further at 150  $\mu$ s than at 170  $\mu$ s, however the velocity in the 150  $\mu$ s case was 14  $\text{m s}^{-1}$  higher than the 170  $\mu$ s example.

As discussed previously, the balls remained lodged in the majority of the solid samples at the velocities used. A post-shot x-ray was taken on one example to establish the final location. For a shot with a velocity of 488  $\text{m s}^{-1}$ , the front of the ball penetrated  $26.5 \pm 0.25$  mm into the mock before stopping. That corresponds to a penetration of  $29.25 \pm 0.25$  mm into the whole sample.

Two images, the 477  $\text{m s}^{-1}$  40  $\mu$ s solid example (Fig. 4 bottom left) and the 40  $\mu$ s ring example (Fig. 5 top left) were selected to compare the image correlation techniques. The aim of this comparison was to reveal any differences between the methods, not to necessarily optimize any particular image or method. Therefore, as closely as possible, the analysis of the output was identical. It is certain that any of the outputs could be improved by specific tweaking of that individual result but this would make overall comparison difficult. In one respect the analysis parameters were forced to differ by the software. The Fourier based codes require the sample boxes to be integer powers of  $2^n$ . The Vic-2D software removes this restriction, but does not allow sample windows greater than  $101 \times 101$  pixels to be used. Table 1 lists the sample window parameters used in the three codes.

Figure 6 shows the three quiver plots for the ball impact on the solid sample. The data filtering in all cases excluded points that had horizontal displacements greater than  $\pm 7$  pixels and  $\pm 6$  pixels vertically. All the algorithms tested here have previously been calibrated and proven against rigid body displacements

**Fig. 6** Quiver plots of the correlation output for the solid sample. Displacement arrows scaled up by 3 for clarity. *Top*, DIC, *middle*, PIV, *bottom*, VIC



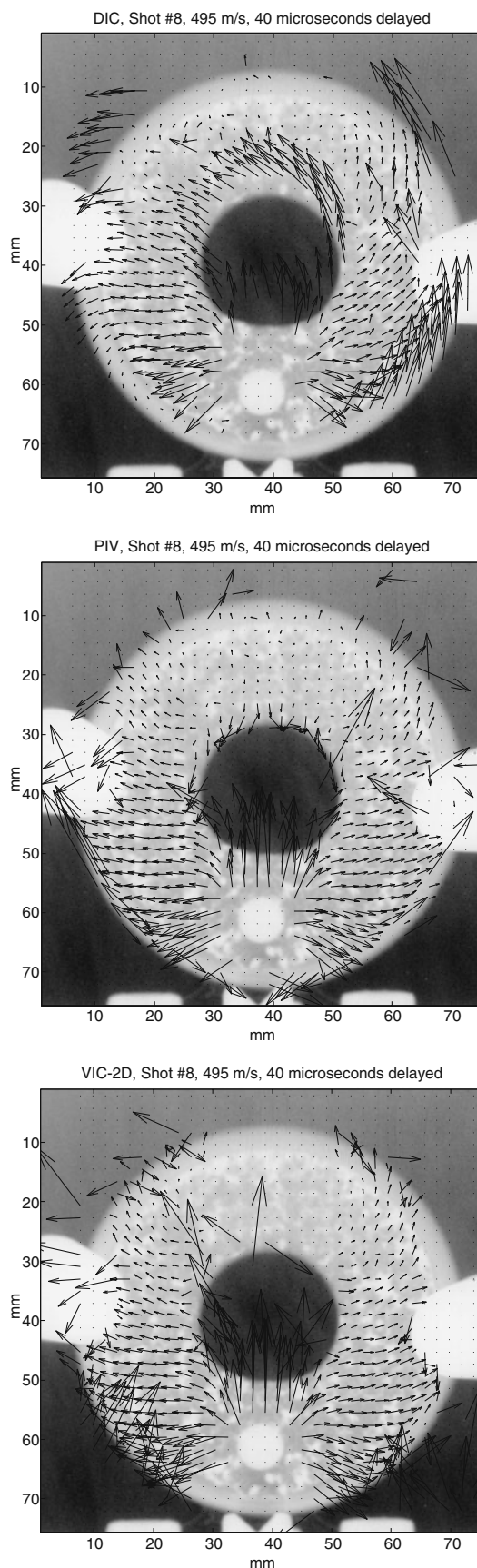
and other tests with known outcomes. It will be seen that there are differences in the results around the case diameter. However, the displacement pattern around the ball is similar from all three methods.

Figure 7 shows the three quiver plots for the ball impact on the ring sample. The data filtering in all cases excluded points that had horizontal displacements greater than  $\pm 10$  pixels and  $\pm 15$  pixels vertically. In this example, the pixel correlation sub-image had approximately a quarter of the information present in the solid sample impact case. This was done because the Vic software failed if a  $101 \times 101$  sub-image was chosen. It will be expected that in a sub-optimal speckle pattern, such as these experiments, the smaller sub-image used will result in higher noise in the displacement estimates. It is observed that the algorithms exhibit much more variability with this set of images than Fig. 6, particularly on the far side of the burn hole.

In optimized speckle patterns, sub-image sizes of  $< 32 \times 32$  pixels are commonly used. This was not possible in these x-ray images owing to the sparse image contrast. Since two of the analysis methods rely on  $2^n$  series to optimize the Fourier transform process, that leaves  $64 \times 64$  and  $128 \times 128$  to be tried. The advantage of the larger sub-image sizes is the greater information content from the low contrast images. The disadvantages are that the local strains are ‘smeared’ into a single value at the center of the sub-image and that the effective data output number is lower. The reduced data density is unfortunate when comparing the experimental values with the computer models.

In an effort to quantitatively compare the three analysis methods, a pair of  $128 \times 128$  images were cropped from an undeformed area of a pre- and post-shot x-ray. The cropped areas were selected by hand to be approximately aligned. In view of the lack of deformation in the area selected, it is expected that the principle difference between the images will be rigid body displacement, excluding the differences inherent to taking and processing two different x-rays. Figure 8 displays the three raw and unprocessed results, together with a composite overlay.

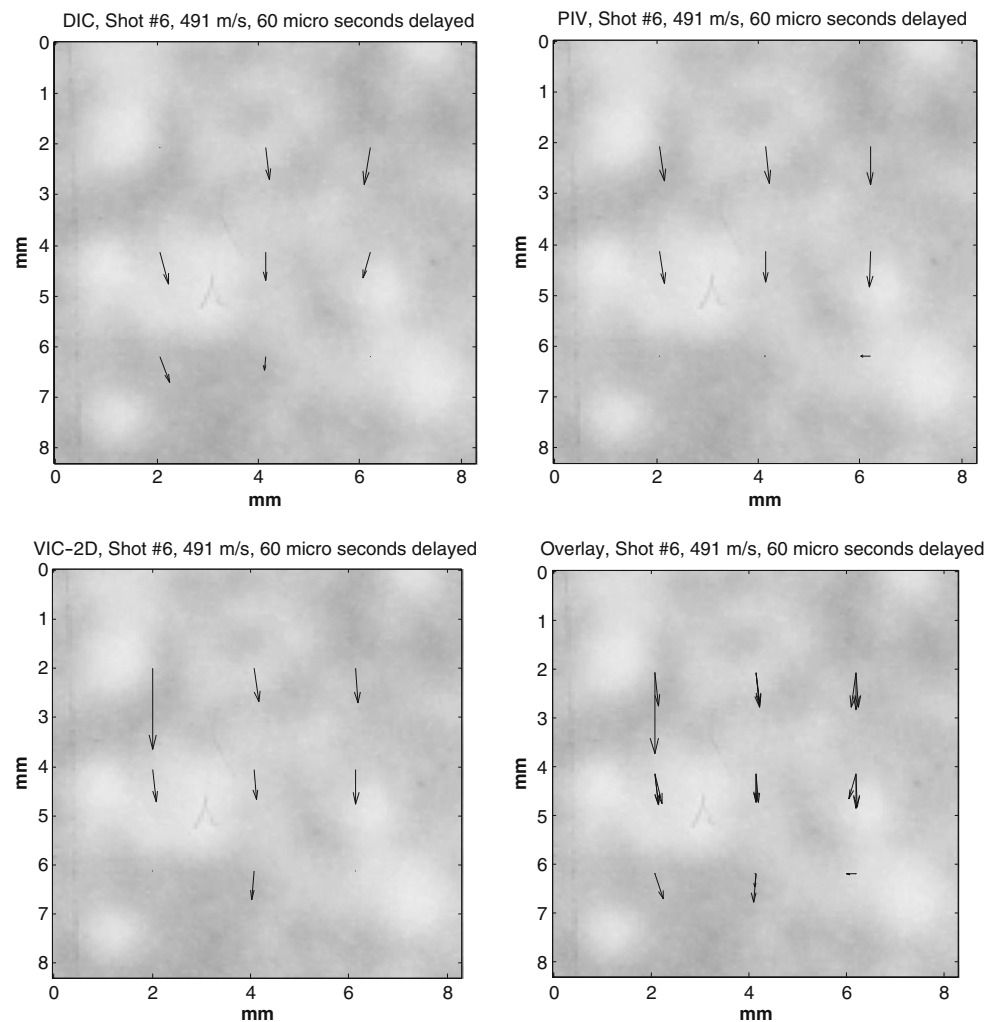
In all cases a  $64 \times 64$  sub-image size ( $63 \times 63$  for the Vic software) spaced 32 pixels apart was used. This gives a maximum of 9 data points for the  $128 \times 128$  pixel image. All three methods failed to find two of the nine correlation points, but they are different



**Fig. 7** Quiver plots of the correlation output for the ring sample. Displacement arrows scaled up by 3 for clarity. *Top*, DIC, *middle*, PIV, *bottom*, VIC



**Fig. 8**  $128 \times 128$  sub-image comparisons. The *bottom right* image displays an overlay of the preceding three. Displacement arrows scaled up by 3 for clarity



for each method. The three methods were in good agreement about the magnitudes of the displacement of the central data point, these numerical results are given in Table 2

## Discussion

It will be observed from Figs. 4 and 5 that the x-ray images are very successful at allowing the position

**Table 2** Displacement values for the central data points in Fig. 8

Code	x displacement (u) / pixels	y displacement (v) / pixels
Vic-2D (1)	0.27	3.11
Sjödahl DIC (2)	0.01	2.93
FFT PIV (3)	0.07	3.14

of the ball within the targets to be identified. In the ring experiments, the lead layer is useful in showing a fraction of the debris cloud crossing the gap, but mock particles without a lead tracer cannot be observed. It will also be noticed that cracking within the mock cannot be detected visually.

The importance of rigid body correction in this experiment can be seen from Fig. 9 where unprocessed and unfiltered displacement data are plotted from the DIC algorithm.

The results from the PIV algorithm (method 3) were generally good and reasonable. Considering Fig. 7, the PIV perhaps produced the most intuitively ‘correct’ plot of the three techniques on this more challenging data set.

The DIC algorithm (method 2) produced the poorest result from the more complex data set (Fig. 7). Not only is there significant residual rotation present, but also

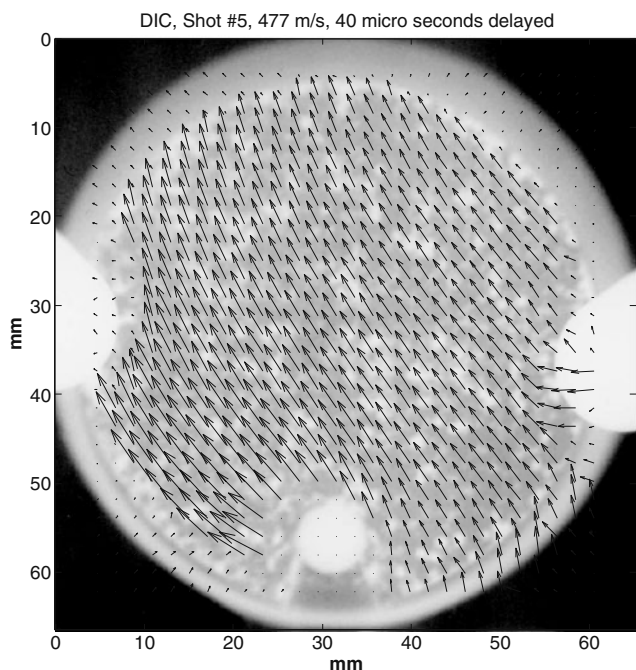


**Fig. 9** Unprocessed output from DIC (method 2) on the solid sample showing the systematic displacements within the mock. Displacement arrows scaled up by 3 for clarity

the data ahead of the projectile is sparser than with the other techniques. It is not clear why this should be given that all the techniques worked adequately on the data shown in Fig. 6.

The Vic-2D program (method 1) also outputted intuitive data in most locations although as with the other methods some clearly ‘bad’ points have made it through the filtering process. An interesting result occurs in Fig. 7 of the ring sample. All the data above the sample hole was bad using the correlation over the whole rectangular image. Unlike the other analysis programs, the Vic software allows the use of circular and polygon masks on the raw images. No doubt had a hollow circular mask been applied the data above the hole would have been adequate. This was not performed because the other analyses were not capable of masking functions.

All three methods gave some displacement data ahead of and around the projectile, however, it was generally sparse presumably owing to the large strains decorrelating the speckle image. The plots all indicate that the displacement was fairly local to the ball on the time scales being recorded here. In theory, the DIC method should not produce extreme outliers because it only searches for a maximum correlation match within the sub-image size. If no suitable match is found, the correlation coefficient is low and it therefore marked as ‘bad’. The small search area is a disadvantage in

cases where large displacements are expected. It also requires the rigid body registration of the image pairs to be fairly close, especially when a small sub-image dimensions are chosen. The PIV software was design with large motions in mind and therefore searches for a possible match over a much wider, and selectable, area. This results in larger potential errors when a false correlation is found. The Vic-2D software also searches more widely for a correlation peak, but it is significantly aided by an initial rigid body guess that is supplied by the user prior to running the program.

It is seen from Table 2 that the quantitative agreement between the three correlation methods is good at the central point. Each method totally failed to find a solution in at least two locations. This is probably due to the proximity of the outer locations to the edge of the image; it is nevertheless interesting that each method had problems at different edge locations. The Vic software had very poor correlation coefficients at all points, as did the PIV technique. The DIC technique had a much wider distribution of correlation coefficients across the image with a very good correlation at the central point and very poor at the top left.

In summary, all three correlation methods produced some valid data from the sub-optimal speckle patterns around the ball impact point in the case of the solid sample, however the results from the burn hole sample were very poor in the ball region for the DIC technique. In all cases the relevant data were sparse in the highly deformed areas owing to the large sub-image size required to allow adequate correlation. The generic filtering routine applied to all the data was inferior in all cases and improvements could easily be made by using an approach that was tailored better to the specific analysis program used.

It has also been shown that using x-rays to track the ball position as a function of time after impact works extremely well. However, it is also evident that the deformation ahead of the projectile is sufficiently localized that the available information from image correlation will be sparse and noisy. These problems render the approach of digital image correlation of x-ray images of localized deformation less than ideal. It had been hoped that extensive crack patterns might have been revealed that could be compared with computer code predictions of such phenomena but this was not found to be the case.

**Acknowledgements** Los Alamos National Laboratory is operated by Los Alamos National Security, LLC, for the NNSA of the U.S. Department of Energy under contract DE-AC52-06NA25396. This research was partially sponsored by the Joint DoD/DoE Munitions Technology Development Program.

## References

1. Hild F, Roux S (2006) Digital image correlation: from displacement measurement to identification of elastic properties—a review. *Strain* 42(2):69–80
2. Sjødahl M (1994) Electronic speckle photography—increased accuracy by nonintegral pixel shifting. *J Appl Opt* 33:6667–6673
3. Schreier HW, Braasch J, Sutton MA (2000) On the systematic errors in digital image correlation. *Opt Eng* 39(11):2915–2921
4. Asay B (2010) Shock wave science and technology reference library, vol 5: non-shock initiation of explosives, 1 edn. Springer
5. Bruck HA, McNeill SR, Sutton MA, Peters WH (1989) Digital image correlation using Newton–Raphson method of partial differential correction. *Exp Mech* 29:261–267
6. Peters WH, Ranson WF (1982) Digital imaging techniques in experimental stress analysis. *Opt Eng* 21:427
7. Peters WH, Ranson WF (1983) Application of digital correlation methods to rigid body mechanics. *Opt Eng* 22:738–742
8. Sutton MA, Wolters WJ, Peters WH, Ranson WF, McNeill SR (1983) Determination of displacements using an improved digital correlation method. *Image Vis Comput* 1:133–139
9. Cheng DJ, Chiang FP, Tan YS, Don HS (1993) Digital speckle-displacement measurement using a complex spectrum method. *Appl Opt* 32(11):1839–1849
10. Eckstein A, Vlachos PP (2009) Digital particle image velocimetry (DPIV) robust phase correlation. *Meas Sci Technol* 20:055,401
11. Sjødahl M (1997) Accuracy in electronic speckle photography. *J Appl Opt* 36:2875–2885
12. Sjødahl M, Benckert L (1993) Electronic speckle photography—analysis of an algorithm giving the displacement with subpixel accuracy. *J Appl Opt* 32:2278–2284
13. Wang YQ, Sutton MA, Schreier HW (2009) Quantitative error assessment in pattern matching: effects of intensity pattern noise, interpolation, subset size and image contrast on motion measurements. *J Strain* 45:160–178
14. White DJ, Take WA, Bolton MD (2003) Soil deformation measurement using particle image velocimetry (PIV) and photogrammetry. *Geotechnique* 53(7):619–631

